MEASUREMENT AND CALCULATION OF ABSOLUTE SINGLE AND MULTIPLE CHARGE EXCHANGE CROSS SECTIONS FOR Feq+ IONS IMPACTING H2O

THE ASTROPHYSICAL JOURNAL, 722:435–439, 2010 October 10 doi:10.1088/0004-637X/722/1/435

MEASUREMENT AND CALCULATION OF ABSOLUTE SINGLE AND MULTIPLE CHARGE EXCHANGE CROSS SECTIONS FOR Fe^{q+} IONS IMPACTING H_2O

J. SIMCIC[1], D. R. SCHULTZ[2], R. J. MAWHORTER[3], J. B. GREENWOOD[4], C. WINSTEAD[5], B. V. MCKOY[5], S. J. SMITH[6], AND A. CHUTJIAN[1]

[1] Atomic and Molecular Physics Group, Jet Propulsion Laboratory/Caltech, Pasadena, CA 91109, USA
[2] Physics Division, Oak Ridge National Laboratory, Oak Ridge, TN 37831-6372, USA
[3] Department of Physics and Astronomy, Pomona College, Claremont, CA 91711, USA
[4] Physics Department, Queen's University, Belfast BT7 1NN, UK
[5] Department of Chemistry, California Institute of Technology, Pasadena, CA 91125, USA
[6] Physics Department, Indiana Wesleyan University, Marion, IN 46953, USA
Received 2010 July 2; accepted 2010 August 9; published 2010 September 21

ABSTRACT

Charge exchange (CE) plays a fundamental role in the collisions of solar- and stellar-wind ions with lunar and planetary exospheres, comets, and circumstellar clouds. Reported herein are absolute cross sections for single, double, triple, and quadruple CE of Fe^{q+} ($q = 5$–13) ions with H_2O at a collision energy of $7q$ keV. One measured value of the pentuple CE is also given for Fe^{9+} ions. An electron cyclotron resonance ion source is used to provide currents of the highly charged Fe ions. Absolute data are derived from knowledge of the target gas pressure, target path length, and incident and charge-exchanged ion currents. Experimental cross sections are compared with new results of the n-electron classical trajectory Monte Carlo approximation. The radiative and non-radiative cascades following electron transfers are approximated using scaled hydrogenic transition probabilities and scaled Auger rates. Also given are estimates of cross sections for single capture, and multiple capture followed by autoionization, as derived from the extended overbarrier model. These estimates are based on new theoretical calculations of the vertical ionization potentials of H_2O up to H_2O^{10+}.

Key words: comets: general – molecular processes – plasmas – solar wind

1. INTRODUCTION

The tremendous progress in detection of X-rays in the solar system (Bhardwaj et al. 2007) has allowed one to understand in finer detail the interactions of the solar wind (SW) and magnetospheric ions with lunar (Robertson et al. 2009) and planetary (Dennerl 2008; Krasnopolsky & Gladstone 2005; Robertson et al. 2009) exospheres, comets (Christian et al. 2010; Cravens 2002; Krasnopolsky et al. 2002; Lisse et al. 1999), the heliosphere (Robertson et al. 2001; Koutroumpa et al. 2009), and the terrestrial magnetosheath (Robertson & Cravens 2003). For SW–comet, SW–heliospheric, and SW–magnetosheath collisions the resulting X-rays can provide a diagnostic of the SW composition, velocity, and flux, as well as the distribution of the neutral gas density in space.

The production of X-rays from SW interactions proceeds through charge exchange (CE) of the heavier, multiply charged ions in the SW with a neutral target. As such, absolute single and multiple CE cross sections are part of the required modeling database that includes the SW ion species, flux, density, velocity, and transition probabilities, together with the target species and density. CE cross sections have been measured for understanding X-ray emissions in comets and atmospheres (see, for example, Greenwood et al. 2000; Čadež et al. 2003; Mawhorter et al. 2007; Djurič et al. 2008; Simcic et al. 2010). Results of theoretical calculations of single and multiple CE cross sections are also available. These calculations are made difficult by the many-electron and (for molecules) multi-center nature of the targets, and uncertainties in the Auger and Coster–Kronig transition rates (Olson et al. 1989; Otranto et al. 2008; Wu et al. 2009; Simcic et al. 2010).

Presented herein are absolute CE cross sections for the species $Fe^{(5–13)+}$ interacting with the cometary and atmospheric H_2O. While Fe ions are only 3% as abundant as oxygen ions in the SW, these heavier species, along with ions of C, N, O, Ne, Mg, Si, and S, give rise to the observed comet and planetary X-ray emissions associated with CE. The experimental approach is summarized in Section 2. Results and comparisons with the multiple or n-electron, classical trajectory Monte Carlo (nCTMC) method and the extended overbarrier model are given in Section 3, and conclusions are given in Section 4.

2. EXPERIMENTAL CONSIDERATIONS

Details of the ion source, beam lines, the CE geometry, gas-cell aperture effects, angular collection efficiency, system calibration, and experimental errors have been given previously (Chutjian et al. 1999; Čadež et al. 2003; Mawhorter et al. 2007; Simcic et al. 2010). Measurements were carried out at an Fe^{q+} energy of $7q$ keV. The ion currents depended on the Fe charge state, and were in the range 4 pA–50 nA.

Separate tests were carried out to search for effects of metastable levels of the projectile ions on the final results (Čadež et al. 2003). In summary, these were (1) generation of Fe^{7+} and Fe^{8+} ions directly from the ECR ion source, (2) subjecting the Fe^{7+} and Fe^{8+} ions to quenching by Ar gas in a section of the beam line, and (3) starting from ECR-extracted Fe^{8+} ions, generating Fe^{7+} by $Fe^{8+} + Ar \rightarrow Fe^{7+} + Ar^{+}$, and Fe^{8+} by $Fe^{9+} + Ar \rightarrow Fe^{8+} + Ar^{+}$. Absolute CE cross sections measured in the collisions with H_2O were the same, within experimental error, for the Fe^{7+} and Fe^{8+} ions produced in (1) and (2), while previous results with Fe^{q+} ions on He (Čadež et al. 2003) showed the same cross sections in (1), (2), and (3). As discussed there, this is compelling evidence that the same starting (ground) state was present in the Fe^{q+} ions. Additionally, in all cases the ECR plasma was operated at a total pressure of greater than $\approx 5 \times$

Table 1
Absolute Single and Multiple CE Cross Sections for $Fe^{(5-13)+}$ Ions Colliding with H_2O

Process	Projectile								
	Fe^{5+}	Fe^{6+}	Fe^{7+}	Fe^{8+}	Fe^{9+}	Fe^{10+}	Fe^{11+}	Fe^{12+}	Fe^{13+}
$\sigma_{q,\,q-1}$	4.14 ± 0.42 4.25	4.82 ± 0.44 4.62	5.24 ± 0.60 5.59	5.05 ± 0.50 6.47	6.70 ± 0.88 7.12	7.71 ± 1.00 7.80	8.60 ± 2.24 8.36	7.99 ± 1.65 8.84	8.56 ± 0.94 9.24
$\sigma_{q,\,q-2}$	1.33 ± 0.28 0.480	1.30 ± 0.22 0.670	1.55 ± 0.34 0.674	1.43 ± 0.31 0.610	1.46 ± 0.43 0.765	1.46 ± 0.40 0.888	1.64 ± 1.44 1.04	1.58 ± 0.91 1.21	1.41 ± 0.38 1.36
$\sigma_{q,\,q-3}$	0.29 ± 0.07 0.169	0.68 ± 0.14 0.206	0.58 ± 0.14 0.241	0.48 ± 0.13 0.208	0.50 ± 0.15 0.234	0.47 ± 0.13 0.252	0.70 ± 0.56 0.278	0.64 ± 0.60 0.338	0.21 ± 0.08 0.427
$\sigma_{q,\,q-4}$	...	0.14 ± 0.03	0.20 ± 0.05	0.23 ± 0.13	0.13 ± 0.05	0.12 ± 0.05	0.06 ± 0.04	...	...
$\sigma_{q,\,q-5}$	...	...	...	...	0.03 ± 0.05	...	...	...	...

Notes. The IP is given in the first column. Projectile energies are $7q$ keV. The second entry in each cell is the calculated cross section in the present nCTMC approximation. See Figures 1–3 for comparisons with error limits on both experimental and theoretical results. All cross sections are in units of 10^{-15} cm^2 and errors are cited at the 2σ level.

10^{-5} Pa, providing additional quenching of Fe^{q+} metastable levels within the plasma (Hossain et al. 2007).

Measurement errors were calculated by adding in quadrature the statistical errors, taking into account the number of measurements for each ion–molecule pair, errors in measuring the gas density, the ion current ratios, absolute currents, the effective gas–cell collision length (corrected for gas streaming), and current fluctuations of the ion beams. The final convoluted 2σ errors in the data are given in Table 1. The averaged errors are 14% ($\sigma_{q,\,q-1}$), 35% ($\sigma_{q,\,q-2}$), 41% ($\sigma_{q,\,q-3}$), and 42% ($\sigma_{q,\,q-4}$).

3. THEORETICAL CONSIDERATIONS

The processes contributing to the measured CE cross sections in collisions of an Fe^{q+} ion with target molecule A-B are given as Fe^{q+} + A-B $\rightarrow Fe^{(q-j)+}$ + A-B$^{(j+s)+}$ + se. Here, $j + s$ is the number of electrons transferred from the target, j is the number of electrons captured by the projectile, and s is the number of free electrons produced by the collision. In the present case, captures up to $j = 5$ have been measured. No determination is made as to whether the A-B$^{(j+s)+}$ species remains as a parent ion, or subsequently decays to excited, fragment ions. One-electron capture occurs mainly to a higher principal quantum number n state of $Fe^{(q-1)+}$ which stabilizes through a series of photon emissions. In the case of two- or three-electron transfers one, two, or three electrons may be in excited states. The resulting excited ion stabilizes either by photon emission or autoionization. For example, single transfer (j+$s = 1$, $s = 0$) and autoionizing double transfer ($j + s = 2$, $s = 1$) will contribute to $\sigma_{q,\,q-1}$. Double transfer ($j = 2$, $s = 0$), single autoionizing triple transfer ($j = 3$, $s = 1$), and double autoionizing quadruple transfer ($j = 4$, $s = 2$) will contribute to $\sigma_{q,\,q-2}$.

The computational method used to calculate the CE cross sections is based on the nCTMC approach (Olson et al. 1989; Schultz et al. 1990). The same procedures used in Simcic et al. (2010) for the Fe^{q+}–CO, CO_2 systems were used here for the Fe^{q+}–H_2O collision pairs in terms of specifying the initial quantum-mechanical electronic probability distributions for position and momentum and for mapping the classical orbital states of the captured electrons to the corresponding quantum states using binning rules (Becker & MacKellar 1983; Raković et al. 2001; Schultz et al. 2001). The target H_2O is considered as a single center with eight active electrons and the interaction between the frozen projectile cores and active target electrons were given by model potentials (Garvey et al. 1975; Schultz & Reinhold 1998) as were those between the electrons and the dominant element (oxygen) in the H_2O target (i.e., each electron interacting with the core through the e–O^+ model potential). The single-center approximation is reasonable at the high collision velocities and Fe^{q+} projectile charge states treated here. The binding energy of the first of the eight electrons in the target is given by the experimentally observed first ionization potential (IP), and that of the next seven electrons by cumulative orbital energies (NIST 2010).

Trajectories for approximately 20,000 projectile-target configurations with a collision energy of $7q$ keV were computed and binned for each of the nine Fe^{q+} ions interacting with H_2O. The resulting events led to one-, two-, three-, four-fold, and five-fold capture, and the quantum states after capture were determined by the non-Coulomb binning method (Schultz et al. 2001). Capture for the higher charges states occurs mainly to about $n = 6$, and to $n = 4$ for the lower charge states, roughly in accord with the usual scaling $n_{\max} \sim q^{3/4}$. The distribution of capture is significant up to about $n = 10$. Single electron capture (SEC) is the largest channel, but double electron capture (DEC), triple electron capture (TEC), and quadruple electron capture (QEC) are significant, and hence one must simulate the ensuing radiative and non-radiative (autoionizing) cascades. This results in a final charge- and quantum-state distribution that would be observed in an experiment where the scattered Fe^{q+} ions have traveled a time prior to detection sufficient for radiative and non-radiative cascades to take place.

Full treatment of these cascades requires quantum-structure and radiative and non-radiative (Auger and Coster–Kronig transition) data for all levels up to $n = 10$ for Fe^{2-11+} (i.e., up to four-fold capture in Fe^{5-13+}). The existing data for these sets of levels and transitions are almost exclusively for low-lying states. Hence as in Simcic et al. (2010), a schematic model of ion quantum levels was created and scaled hydrogenic transition probabilities and scaled Auger rates were used (see, e.g., Burgdörfer et al. 2003). Cascades were computed for double, triple, and quadruple capture events in a multiply excited state using a conventional treatment of multiple Auger electron emission and fluorescence in plasmas (see, e.g., Kaastra & Mewe 1993). Estimates are given below as to the uncertainty of final calculated results arising from approximations in the cascade models.

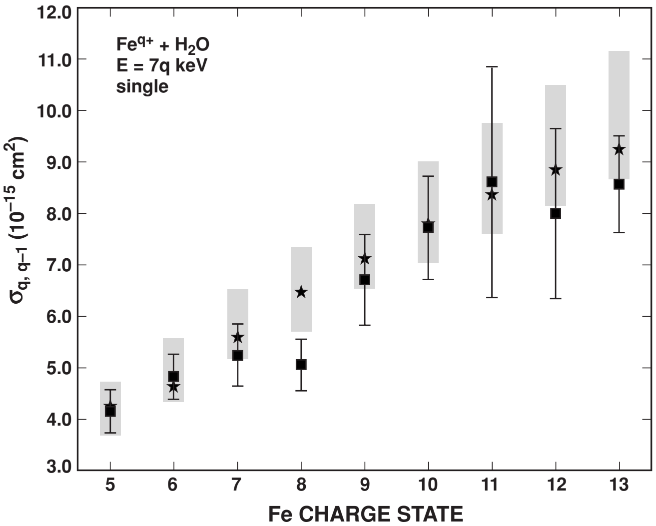

Figure 1. Results of the *n*CTMC calculation and radiative/Auger cascade processing for CE in Fe^{5-13+} collisions with H_2O (★) compared with the present experiments (■). Shown are the single CE results with error bars representing the maximum estimated uncertainty from the cascade model. See also data listings in Table 1.

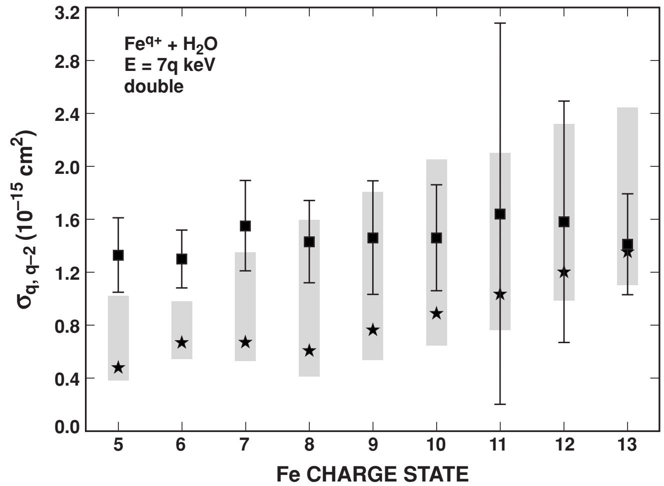

Figure 2. Same as for Figure 1, but for the double CE results.

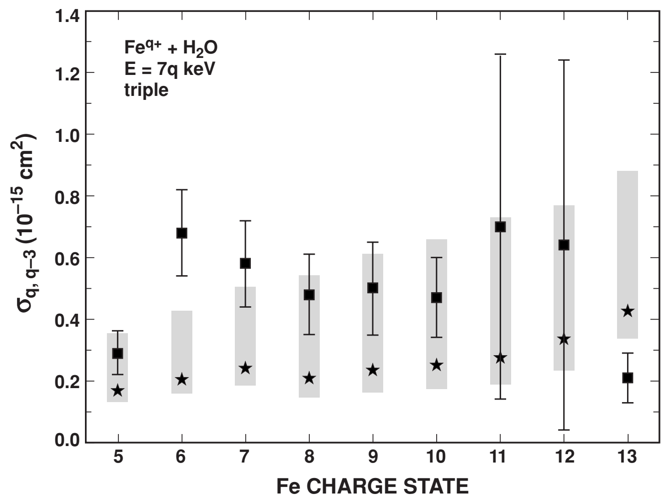

Figure 3. Same as for Figure 1, but for the triple CE results.

4. RESULTS AND DISCUSSION

Absolute single ($\sigma_{q,\,q-1}$), double ($\sigma_{q,\,q-2}$), triple ($\sigma_{q,\,q-3}$), quadruple ($\sigma_{q,\,q-4}$), and (one) pentuple ($\sigma_{q,\,q-5}$) CE cross sections for the Fe^{q+} ions colliding with H_2O are listed in Table 1. Results of the *n*CTMC calculation and the radiative/Auger cascade processing for the nine iron ions colliding with H_2O are also listed in Table 1, and shown in Figure 1 (SEC), Figure 2 (DEC), and Figure 3 (TEC). The error limits associated with the theoretical results are estimates of the minimum and maximum contributions possible from the cascade process. As with CO and CO_2, (Simcic et al. 2010), the maximum is given by the calculated direct SEC cross section, plus 100% of the DEC and estimated maximum fractions of the TEC and QEC undergoing cascade added to the SEC result. The minimum is given by assuming complete stabilization of the multiple electron capture computed by *n*CTMC in the DEC, TEC, and QEC channels. These represent the extremes of the contributions from cascades that could raise or lower the SEC results. Similarly for DEC, the maximum is found by adding to the direct *n*CTMC DEC cross section the estimated largest contributions from TEC and QEC, and the minimum by assuming complete stabilization of the TEC and QEC inputs to the cascade. The same approach is used to estimate cascade errors for TEC. It should be noted that these uncertainties are inherent to the cascade following the initial multiply excited population from that calculation and not to approximations in the *n*CTMC model which has its own uncertainties in producing the input distribution of populated levels for the cascade model.

Good agreement of the theoretical results with the measurements is seen. In particular, the magnitude and trend of the results for SEC agree very well with the measurements for both the lower and higher *q*'s. The *n*CTMC and experimental results for SEC display a smooth trend, with the possible exception of the Fe^{8+} results that may reflect details not included in the collision or cascade models. The theoretical results for DEC also agree well with measurements in that they are both nearly constant for all charge states, but the theoretical data are about a factor of 2–3 smaller in magnitude, as with previous results for the CO and CO_2 targets, and the *n*CTMC + cascade results for TEC are nearly flat (Simcic et al. 2010). Results are in qualitative agreement with experiment, given the larger experimental errors associated with the smaller TEC cross sections. The rising trend of the SEC cross section with increasing *q* is the result of the projectile's presenting a larger capturing sphere or impact parameter *b* for the higher charge states. For SEC this occurs over a wide range of *b*, with the probability for capture peaking at small *b*. For DEC and TEC which occur over a smaller range of *b*, increases in *q* do not increase the multiple capture probability as much as they can for SEC which has a smaller probability for capture that extends to larger *b*, yielding the much flatter dependence as a function of *q*.

Finally, the semiempirical extended overbarrier model (EOBM; Niehaus 1987) was used in a calculation of the relative fraction of the true capture channel versus autoionizing multiple capture channel for H_2O. This is the analogous approach used for the calculation of CO and CO_2 cross sections for projectile $Fe^{(5-7)+}$ ions (Simcic et al. 2010). Vertical IPs up to H_2O^{10+} are required for calculating the various barrier heights and transition probabilities of electron capture by the target and projectile states. These IPs were calculated as differences between the ground-state energy of neutral H_2O and the ground-state energies of ions having the same nuclear

Table 2
Calculated Vertical Ionization Potentials for H_2O

Charge State	Symmetry	Energy (eV)
H_2O^{1+}	$^2B_1$	12.46
H_2O^{2+}	$^3B_1$	39.8
	$^1A_1$	41.0
H_2O^{3+}	$^2A_1$	84.8
	$^4A_2$	85.2
H_2O^{4+}	$^3B_2$	148.2
	$^1A_1$	149.2
H_2O^{5+}	$^2B_2$	233.1
H_2O^{6+}	$^1A_1$	341.7
H_2O^{7+}	$^2A_1$	485.5[a]
H_2O^{8+}	$^1A_1$	655[b]
H_2O^{9+}	$^2A_1$	1423[b]
H_2O^{10+}	...	2323[c]

Notes.
[a] Results from the restricted open-shell Hartree–Fock calculation with multi-reference single–double configuration-interaction (ROHF+MR-SDCI).
[b] Results from the Hartree–Fock calculation.
[c] As calculated from the difference between the total energy of neutral H_2O and Coulomb repulsion energy of the bare nuclei.

geometry, using the electronic-structure package GAMESS (Schmidt et al. 1993). All calculations used the so-called augmented correlation-consistent polarized valence double-zeta (aug-cc-pVDZ) basis set (Dunning 1989) as contained in GAMESS. The geometry of the neutral ground state was optimized in the C_{2v} point group using a "complete active space" multiconfigurational self-consistent-field wave function in which the eight valence electrons were allowed to occupy eight orbitals in all possible ways, a type of calculation commonly designated (8,8)CASSCF. The resulting geometry, with r(O–H) = 0.9687 Å and $\angle$(H–O–H) = 103°.97, was used in all subsequent calculations. For reference, Császár et al. (2005) found the equilibrium values r(O–H) = 0.9578 Å and $\angle$(H–O–H) = 104°.48 to be consistent with spectroscopic data. The neutral ground-state energy was determined from a multireference configuration interaction (MRCI) calculation that included all single and double excitations from the (8,8)CASSCF active space. Energies for ionizations up to H_2O^{7+} were determined from similar MRCI calculations based on ionic CASSCF reference wave functions. For a consistent quality of description, the number of CASSCF active orbitals was held fixed at eight, so that the reference function for the q+ ion was $(8-q, 8)$CASSCF, while the 8+ and 9+ energies were computed at the Hartree–Fock level. The 10+ energy is simply the difference between the total MRCI energy of the neutral and the Coulomb repulsion energy of the bare nuclei.

Calculated IPs are listed in Table 2. The IPs for the lowest three ionization states compare well to previous values. The calculated value of 12.46 eV for ionization to the $^2B_1$ ground state of H_2O^+ differs by 0.16 eV from the recommended vertical IP of 12.62 eV (NIST 2010). The vertical IP of 39.8 eV for reaching the $^3B_1$ ground state of H_2O^{2+} is in agreement with the value of 39.76 eV calculated directly using the two-electron Dyson propagator (Ida & Ortiz 2008). For the $^2A_1$ ground state of H_2O^{3+}, the vertical IP of 84.8 eV is within 0.2 eV of the value, 84.60 eV, calculated from the three-particle propagator (Handke et al. 1995). No other results appear to be available for the more highly charged ions. Results of the EOBM approximation for H_2O and $Fe^{(5-13)+}$ for all excitation strings are shown in Figure 4. One sees that the auotoionizing transfers make a wide-ranging, 0%–70% contribution to the CEs for the measured charge states Fe^{5+} to Fe^{13+}.

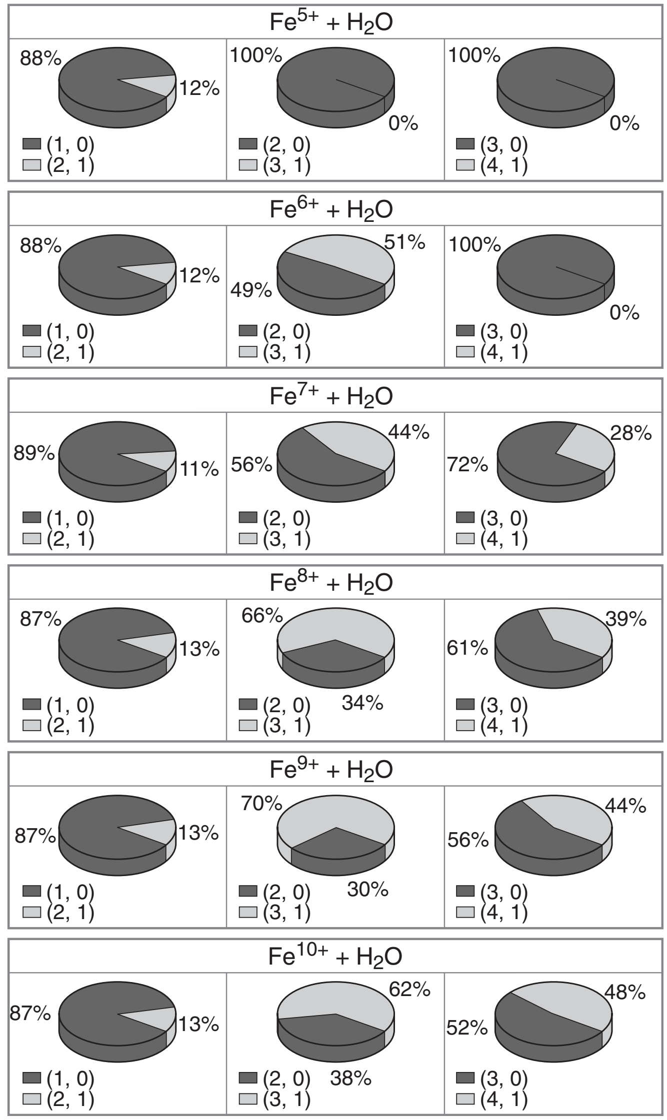

Figure 4. Pie chart representing the fractions of true capture and autoionizing multiple captures for $Fe^{(5-13)+}$ ions with H_2O, as calculated in the extended overbarrier model. The legend $(j + s, s)$ refers to j+s electron transfers followed by s electron autoionizations.

5. CONCLUSIONS

Comparisons have been presented between experimentally measured absolute CE cross sections and the nCTMC approximation for collisions of $Fe^{(5-13)+}$ ions with H_2O. Experimental and theoretical results for capture of up to three electrons are given, as well as experimental data for many four- and one five-electron capture cases. There is agreement within combined experimental and theoretical error limits for $\sigma_{q,\, q-1}$, and agreement within error limits in most cases for the smaller cross sections $\sigma_{q,\, q-2}$ and $\sigma_{q,\, q-3}$. In addition, the EOBM was used to estimate the fraction of true captures and autoionizing multiple captures in the CE process. Accurate IPs required for up to H_2O^{10+} in the EOBM estimates were calculated using the electronic structure package GAMESS and MRCI. The results presented provide CE cross sections for the SW-abundant

Fe ions and the comet-abundant species H_2O that are useful in astrophysical simulations as well as providing theoretical insight into the capture and autoionization processes.

The experimental work was carried out at JPL/Caltech, and was supported by the National Aeronautics and Space Administration through agreement with the California Institute of Technology. D.R.S. gratefully acknowledges support from the US Department of Energy under Contract No. DE-AC05-OR22464.

REFERENCES

Becker, R. L., & MacKellar, A. D. 1983, J. Phys. B: At. Mol. Opt. Phys., 17, 3923
Bhardwaj, A., et al. 2007, Planet. Space Sci., 55, 1135
Burgdörfer, J., Reinhold, C. O., & Meyer, F. 2003, Nucl. Instrum. Methods Phys. Res. B, 205, 690
Čadež, I., Greenwood, J. B., Lozano, J. A., Mawhorter, R. J., Smith, S. J., Niimura, M., & Chutjian, A. 2003, J. Phys. B: At. Mol. Opt. Phys., 36, 3303
Christian, D. J., et al. 2010, ApJS, 187, 447
Chutjian, A., Greenwood, J. B., & Smith, S. J. 1999, in AIP Conf. Proc. 475, Applications of Accelerators in Research and Industry, ed. J. L. Duggan & I. L. Morgan (Melville, NY: AIP), 881
Cravens, T. E. 2002, Science, 296, 1042
Császár, A. G., Czakó, G., Furtenbacher, T., Tennyson, J., Szalay, V., Shirin, S. V., Zobov, N. F., & Polyansky, O. L. 2005, J. Chem. Phys., 122, 214305
Dennerl, K. 2008, Planet. Space Sci., 56, 1414
Djurič, N., Smith, S. J., Simcic, J., & Chutjian, A. 2008, ApJ, 679, 1661
Dunning, T. H. 1989, J. Chem. Phys., 90, 1007
Garvey, R. H., Jackman, C. H., & Green, A. E. S. 1975, Phys. Rev. A, 12, 1144
Greenwood, J. B., Williams, I. D., Smith, S. J., & Chutjian, A. 2000, ApJ, 533, L175
Handke, G., Tarantelli, F., Tarantelli, A., & Cederbaum, L. S. 1995, J. Electron Spectrosc. Relat. Phenom., 75, 109
Hossain, S., Tayal, S. S., Smith, S. J., Raymond, J. C., & Chutjian, A. 2007, Phys. Rev. A, 75, 022709
Ida, T., & Ortiz, J. V. 2008, J. Chem. Phys., 129, 084105
Kaastra, J. S., & Mewe, R. 1993, A&AS, 97, 443
Koutroumpa, D., Lallement, R., Kharchenko, V., & Dalgarno, A. 2009, Space Sci. Rev., 143, 217
Krasnopolsky, V. A., & Gladstone, G. R. 2005, Icarus, 176, 395
Krasnopolsky, V. A., et al. 2002, Icarus, 160, 437
Lisse, C. M., et al. 1999, Earth Moon Planets, 77, 283
Mawhorter, R. J., et al. 2007, Phys. Rev. A, 75, 032704
Niehaus, A. 1987, Nucl. Instrum. Methods Phys. Res. B, 23, 17
NIST 2010, NIST Chemistry Webbook (Gaithersburg, MD: NIST), http://webbook.nist.gov
Olson, R. E., Ullrich, J., & Schmidt-Böcking, H. 1989, Phys. Rev. A, 39, 5572
Otranto, S., Olson, R. E., & Beiersdorfer, P. 2008, Can. J. Phys., 86, 171
Raković, M. J., Schultz, D. R., Stancil, P. C., & Janev, R. K. 2001, J. Phys. A: Math. Gen., 34, 4753
Robertson, I. P., & Cravens, T. E. 2003, J. Geophys. Res., 108, 6
Robertson, I. P., Cravens, T. E., Snowden, S., & Linde, T. 2001, Space Sci. Rev., 97, 401
Robertson, I. P., et al. 2009, Geophys. Res. Lett., 36, L21102
Schmidt, M. W., et al. 1993, J. Comput. Chem., 14, 1347
Schultz, D. R., Olson, R. E., Reinhold, C. O., Kelbch, S., Kelbch, C., Schmidt-Böcking, H., & Ullrich, J. 1990, J. Phys. B: At. Mol. Opt. Phys., 23, 3839
Schultz, D. R., & Reinhold, C. O. 1998, Comput. Phys. Commun., 114, 342
Schultz, D. R., Stancil, P. C., & Raković, M. J. 2001, J. Phys. B: At. Mol. Opt. Phys., 34, 2739
Simcic, J., Schultz, D. R., Mawhorter, R. J., Čadež, I., Greenwood, J. B., Chutjian, A., Lisse, C. M., & Smith, S. J. 2010, Phys. Rev. A, 81, 062715
Wu, Y., Qi, Y. Y., Zou, S. Y., Wang, J. G., Li, Y., Buenker, R. J., & Stancil, P. C. 2009, Phys. Rev. A, 79, 062711